Heat-affected zone and ablation rate of copper ablated with femtosecond laser

Yoichi Hirayama and Minoru Obara[a)]
Department of Electronics and Electrical Engineering, Keio University, 3-14-1 Hiyoshi, Kohoku-ku, Yokohama 223-8522, Japan

(Received 17 September 2004; accepted 30 November 2004; published online 1 March 2005)

We describe the experimental and molecular dynamics simulation study of crystalline copper (Cu) ablation using femtosecond lasers. This study is focused on the heat-affected zone after femtosecond laser ablation and the laser ablation rate. As a result of the x-ray diffraction measurement on the ablated surface, the crystallinity of the surface is partially changed from a crystal structure into an amorphous one. At the laser fluences below the ablation threshold, the entire laser energy coupled to the Cu target is absorbed, while during the fluence regime over the threshold fluence, the ablation rate depends on the absorption coefficient, and the residual energy which is not used for the ablation, is left in the Cu substrate. The heat-affected zone at the fluences below the threshold is estimated to be greater than that over the threshold fluence. In addition, the laser ablation of Cu is theoretically investigated by a two-temperature model and molecular dynamics (MD) simulation to explain the heat-affected zone and ablation rate. The MD simulation takes into account the electron temperature and thermal diffusion length calculated by the two-temperature model. Variation in the lattice temperature with time and depth is calculated by the MD simulation coupled with the two-temperature model. The experimental ablation rate and the heat-affected zone are theoretically well explained. © *2005 American Institute of Physics*. [DOI: 10.1063/1.1852692]

I. INTRODUCTION

The intense ultrashort pulsed laser interaction with metals is a subject of practical interest as well as material science interest. Significant advancements in broadband solid state lasers and the chirped pulse amplification technique using Ti:sapphire, Cr:LiSAF, and Cr:LiCAF laser media have led to the challenging phase of this research. The application fields include high-intensity physics,[1] ultrashort pulsed laser ablation,[2,3] high order harmonics generation,[4] and so on. Femtosecond laser ablation is one of the most promising technologies among the femtosecond laser applications because ablation physics is drastically different from those of conventional nanosecond and longer pulsed laser ablation. Generally, the electron-lattice relaxation time in metals is 1–10 ps.[5,6] Therefore, the mechanism of femtosecond laser ablation is different from that of longer pulsed laser ablation. Thermal ablation occurs when the laser pulsewidth is longer than the electron-lattice relaxation time. The importance of the laser pulsewidth compared to the electron-lattice relaxation time and the thermal diffusion length in relation to the optical skin depth has been pointed out.[7]

As for metal ablation, theoretical investigations[8–10] on the short pulse laser ablation of metals have been reported. The femtosecond laser ablation is numerically simulated using a two-temperature mode,[8,9] and the heat conduction equation of Au and Si.[10] The molecular dynamics (MD) simulation is mainly used to describe the physical phenomena of the interaction of ultrashort laser pulses with different materials[11–15] and rarely to evaluate the ablation depth in nickel[16] and laser melting of Ni and Au films.[17] Moreover, the femtosecond laser ablation of materials with a high thermal conductivity is of paramount importance,[9,18,19] because the chemical composition and properties of the ablated area after the femtosecond laser ablation remains unchanged.[19–22] The material processing using femtosecond lasers can well control the heat-affected zone of dielectric and semiconductor materials. Regarding the femtosecond laser ablation of metals, the residual energy left in the metal, which is not used for ablation, induces a liquid phase, leading to the amorphous or polycrystalline phase of the metal during resolidification. Previously, the heat transfer in metals irradiated with subpicosecond laser pulses is theoretically simulated based on the two-temperature diffusion model,[23] and the ablation rate of aluminum has been studied using a developed simulation code.[24] In the case of gold, it was experimentally demonstrated that a very small heat effect exists after the femtosecond laser irradiation.[25]

In this article, we experimentally estimate the heat-affected zone of the metallic bulk crystal of copper (Cu) after femtosecond laser ablation, and also theoretically explain the ablation characteristics of Cu irradiated with a femtosecond laser using the MD simulation. Cu is recently a very important conductor in the large scale integration. To repair the conductor wiring and customize the circuits, the femtosecond laser ablation is used. It is very important to know the characteristics of the femtosecond laser ablation and the heat-affected zone of Cu. The x-ray diffraction (XRD) measurements and argon ion etching are performed one after another at the area ablated by the femtosecond laser in order to estimate the thickness of the heat-affected zone. The crystallinity on the ablated area is found to partially change into

[a)]Author to whom correspondence should be addressed; electronic mail: obara@obara.elec.keio.ac.jp

an amorphous form. The thickness of the heat-affected zone is estimated to be 0.5–3.5 μm, dependent on the laser fluence. The electron excitation by the femtosecond laser calculated by two-temperature model is taken into account in the MD simulation model. The ablation rate and the heat-affected zone are theoretically well explained.

II. THEORETICAL MODEL

A. Two-temperature model

The models used in our simulation to describe the laser ablation of Cu are the two-temperature model and two-dimensional (2D) MD simulation model. In the case of the femtosecond laser ablation of metals, the laser energy is absorbed by the conduction electrons. The electron dynamics by ultrafast laser excitation has been discussed by Anisimov *et al.*,[26] who proposed that the electron gas temperature could follow the temporal shape of the laser pulse because the specific heat of the degenerate electrons is very small. The heating process of the lattice system cannot follow the laser temporal shape due to the large mass of ions compared to that of the electrons. Therefore, the entire system reaches thermal equilibrium after energy relaxation from the electrons to the lattice system.

In order to describe this phenomenon, the two-temperature model is widely used.[8,9,18] This model takes into account the energy relaxation between electrons and phonons and the thermal diffusion, i.e., Fourier law, as follows:

$$C_e\frac{\partial T_e}{\partial t} = \mathrm{div}(\kappa_e \nabla T_e) - \varsigma(T_e - T_i) + Q,$$

$$C_i\frac{\partial T_i}{\partial t} = \varsigma(T_e - T_i), \tag{1}$$

$$Q = (1-R)\alpha q(t)\exp[-\alpha z],$$

where C, κ, and T are the heat capacity, thermal conductivity, and temperature, respectively. The subscripts e and i denote the electron system and lattice system, respectively. Q is the energy absorbed by the laser irradiation. $q(t)$, R, α, and ζ are the time-intensity pulse-shape function, reflectivity, optical absorption coefficient, and the electron–lattice coupling coefficient, respectively. The correction of parameters (C_e, κ_e, and ζ) at room temperature have been introduced.[27] Although it is possible to numerically solve Eq. (1), it is known that the two-dimensional analytical solution, in which κ and α are assumed to be constant, is a good approximation.[18]

In the case of low fluence ablation, it has been considered that the number density of hot electrons is so low that energy transfer occurs only within the area characterized by the skin depth $d=1/\alpha$. However, in the case of a high enough laser fluence, the electron thermal diffusion length, $l=\sqrt{D\tau_a}$, becomes significant, where D is the thermal diffusion coefficient, $D=\kappa_e/C_e$, and τ_a is expressed as

$$\tau_a = \frac{\tau_e t_p(t_p+\tau_i)}{\tau_e(t_p+\tau_i)+t_p\tau_i} + \frac{\tau_e\tau_i}{\tau_e+\tau_i}, \tag{2}$$

where $\tau_e=C_e/\gamma$, $\tau_i=C_i/\gamma$, and t_p are the electron cooling time, the lattice heating time, and laser pulse width, respectively, and γ is a parameter which characterizes the electron–lattice coupling.[9] The electron excitation and the electron thermal diffusion length are taken into account when the laser energy is absorbed in the Cu target in the MD simulation.

B. Molecular dynamics simulation

The model developed to describe the laser ablation of Cu is the 2D molecular dynamics model for Ni.[16] The standard molecular dynamics simulation technique is used to investigate the ablation process. The numerically stable and simple velocity Verlet algorithm[28] is used to investigate the equation of motion. The interaction between atoms in the system is described by the following Morse potential of the face-centered cubic metal and its particular parameter for Cu are taken from Ref. 29

$$\phi(r) = D[\exp\{-2\alpha(r-r_0)\} - 2\exp\{-\alpha(r-r_0)\}], \tag{3}$$

where D is 0.3429 eV, α is 1.359 Å^{-1}, and r_0 is 2.866 Å.[30]

If the distance between atoms becomes longer than the balanced distance r_0, the interaction between atoms is neglected. Therefore, it does not calculate the interaction between atoms having a distance exceeding the cutoff distance, which is five times the balanced distance.

The computational system is formed by a certain number of unit face-centered cubic cells and has the dimensions of $x=14$ nm and $z=200$ nm (4.8×10^4 particles). It is assumed that the direction of the x axis has almost no information in order to reduce the calculation load. The particles at the boundary have arranged the fixed atoms into three layers of the direction with both ends of an x axis in the target, and have arranged the velocity scaling layer into three layers of the inner side. The z axis termination has three arranged layers of fixed atoms. Moreover, the velocity scaling layer has been arranged into three layers of the inner side in order to suppress the shock wave radiation. The upper layer from the z-axis surface is dealt with as a vacuum and arranges no particles. The initial temperature, which is 300 K, is used by the system as the transformed velocity vector. The direction and the size of the velocity are given by random numbers and the following equation, respectively,

$$\left\langle \frac{mv^2}{2} \right\rangle = \frac{3}{2}k_B T, \tag{4}$$

where m, v, k_B, and T are the particle mass, velocity, Boltzmann constant, and temperature, respectively.

The laser interaction with Cu is simulated for laser pulsewidth of $t_p=200$ fs at the wavelength of 800 nm. The laser beam intensity is spatially a rectangular shape and has a Gaussian temporal distribution. The laser energy is exponentially deposited into the material in z direction following Lambert–Beer's law.

Laser energy is directly given to the particles as the transformed velocity which has a random direction. After the

TABLE I. Physical constants of copper used in the simulation. R is percent reflection and α is optical absorption coefficient.

R (%)	α (cm^{-1})	C_e ($J/cm^3\,K^2$)	C_i ($J/cm^3\,K$)	κ (W/mK)	γ ($GW/cm^3\,K$)	T_m (K)	T_b (K)
96	8.36×10^5	97	3.46×10^6	401	700	1356	2811

end of the laser irradiation, the particles move according to the atomic force calculated by the Morse potential, and the results are obtained as the coordinates, velocity, and acceleration by numerical integration using the Verlet method. Although the parameters of the particles that absorbed the laser energy actually start to change from the onset of the laser irradiation, these time variations are not taken into consideration in this article, because the contribution of the electrons is dominant during the laser irradiation and the electron excitation is taken into account in the two-temperature model calculation.

The experimental data for the ultrashort laser ablation of metals[9,18] show the presence of two different ablation regimes. The number density of the hot electrons is very low at low fluences. Consequently, the energy transfer from the electrons to the lattice occurs only within the skin depth d characterized by the optical absorption coefficient. On the other hand, the electron thermal diffusion length l becomes significant at higher fluences and it increases the ablation rate. These effects, which are calculated by the two-temperature model, are also taken into account in the MD simulation model.

The parameters used in the simulation are listed in Table I.[9,27,31]

III. EXPERIMENTAL PROCEDURE

The laser used in our experiment is a titanium–sapphire laser with a chirped pulse amplification system pumped by the second harmonic of a Nd:YLF laser at a 1 kpps repetition rate. The pulsewidth, the center wavelength and pulse energy are 100 fs, 800 nm, and 1 mJ, respectively. The intensity autocorrelator and the powermeter at the exit of the amplifier periodically monitored the drifts in the pulse width and output energy in order to ensure a stable pulse energy on the Cu target. To control the pulse energy, we used optical neutral density filters. An 80 mm focal length fused silica convex lens is used to focus the attenuated laser pulses onto the Cu substrate. The irradiation number of laser pulses is controlled by a mechanical shutter. The sample is a metallic bulk of Cu, whose crystallinity is polycrystalline. All the ablation experiments were performed in air at room temperature. The ablation depths after laser ablation are measured using a mechanical stylus (Dektak-3030). The ablation rate is estimated as an averaged value over 300 subsequent pulses. After the ablation experiments, the crystallinity of the ablated area is measured using XRD (Rigaku RAD-C). In order to estimate the thickness of the heat-affected zone, we perform the XRD measurements of the ablated bottom area after etching with an argon ion etching apparatus (JEOL, Ltd., Model 9000-MC).

IV. RESULTS AND DISCUSSION

A. Experimental results of heat-affected zone measurement

The measurement procedure of the heat-affected zone after an intense femtosecond laser irradiation is precisely described in Ref. 25. We first investigated the etching rate of the argon ion etching apparatus used in this experiment, which is calculated to be 0.1005 μm/min. Next, in order to estimate the thickness of the heat-affected zone, the laser-ablated area which is etched using the argon ion etching apparatus, is measured by XRD. It is not changed at the sample surface, although the surface of the Cu sample etched by the argon ions is measured using XRD whether or not the XRD peak signals are changed by etching.

The Cu(2 0 0) XRD signals from the ablated area at the laser fluence of 1.04 J/cm^2 after Ar^+ etching are shown in Fig. 1. The XRD peak signals of the bottom area ablated with the femtosecond laser are found to be weaker than that of the crystalline sample. However, the full width at half maximum of the XRD signal is unchanged even after the argon ion etching. Additionally, the XRD wide scan measurements in both cases of the sample which is not etched and the ablated area at the laser fluence of 1.04 J/cm^2, which is etched for 36 min after the laser ablation, are shown in Figs. 2(a) and 2(b). The Cu sample used in this experiment is polycrystalline because it has some large peak signals. The XRD signals from the ablated area after etching become almost the same as that of the sample, as shown in Fig. 2. Although the crystallinity of the Cu sample used is polycrystalline before the laser ablation, the crystallinity of the ablated area is partially changed into amorphous. The residual energy absorbed that was not used for the ablation process remains, leading to the formation of a thin melt phase layer.

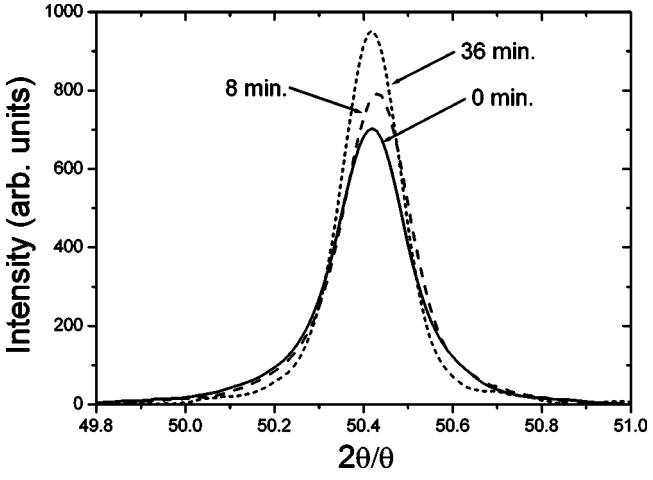

FIG. 1. Variation of XRD narrow scan of Cu(2 0 0) in the ablated area with etching time. Laser fluence is 1.04 J/cm^2.

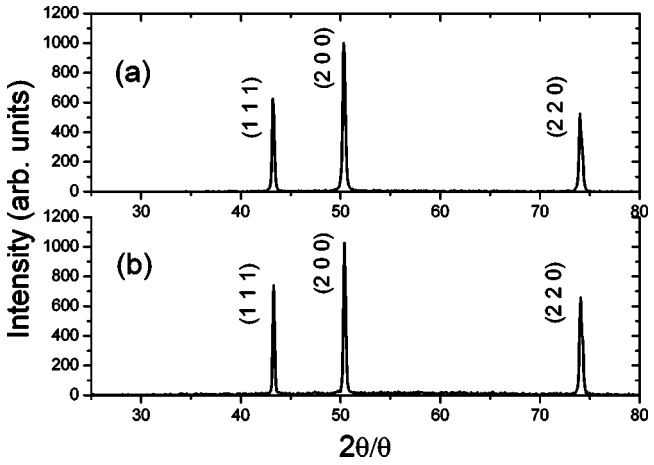

FIG. 2. XRD wide scan measurements for both (a) sample which is not etched and (b) the ablated area at the laser fluence of 1.04 J/cm^2 which is etched for 36 min after laser ablation.

The dependence of the XRD peak intensity on the etching time for the Cu sample and the ablated area is shown in Fig. 3. While the XRD peak intensity of the Cu sample has hardly any changes, the XRD peak intensity of the bottom area ablated with a femtosecond laser at three laser fluences are found to be weaker than that of the crystalline sample. The melt layer is abruptly cooled down and recrystallized, but is amorphous. It is evident that the area ablated by the femtosecond laser is converted into an amorphous metal. This mechanism would be similar to the melt quenching generally used as the fabrication method of amorphous metals.

The XRD peak intensity after Ar^+ etching gradually increases and then becomes saturated. The saturated value of the XRD peak intensity is close to the XRD peak intensity of the Cu sample. Therefore, the amorphous layer fabricated by laser ablation is completely removed by etching, and the crystalline region appears on the etched surface. The thickness of the amorphous layer is evaluated from the argon ion etching rate and etching time shown in Fig. 3. The estimated amorphous layer, in other words, the heat-affected zone, is

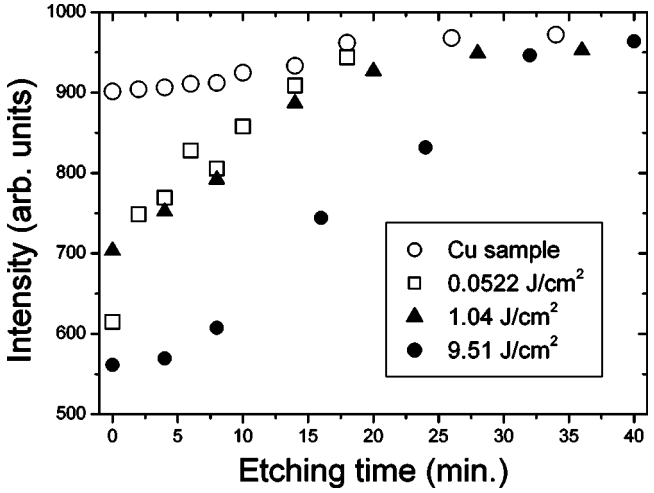

FIG. 3. Plots of the XRD peak intensity of sample and the ablated area as a function of etching time: (○) Cu sample,(□) 0.0522 J/cm^2, (▲) 1.04 J/cm^2, (●) 9.51 J/cm^2.

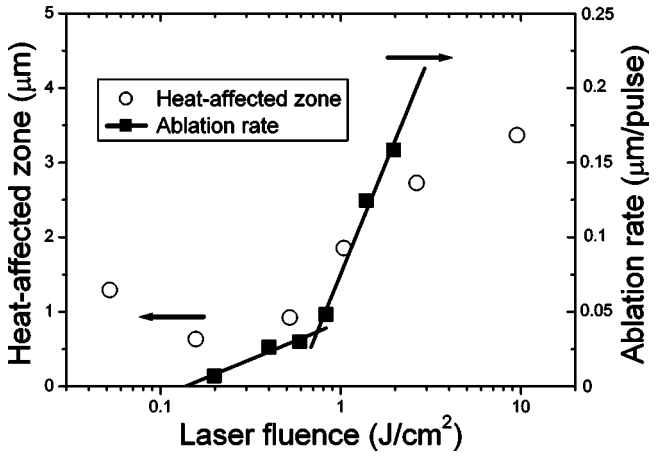

FIG. 4. Dependence of the estimated thickness of heat-affected zone and the experimental ablation rate on the laser fluence.

shown in Fig. 4. Additionally, the ablation rate of Cu is also shown in Fig. 4. At the fluence of 0.0522 J/cm^2, which is below the ablation threshold fluence of 0.137 J/cm^2, the entire fluence coupled to the Cu target is absorbed because the laser ablation does not occur. While at the low fluence regime over the threshold fluence, the ablation rate depends on the absorption coefficient, and the residual energy, which is not used for the ablation is left. Therefore, the thickness of the heat-affected zone at laser fluences below the threshold is greater than that in the low fluence regimes. For the high fluence regime, the ablation rate depends on the thermal diffusion length and the thickness of the heat-affected zone is greater because the laser energy is absorbed into the deep layer due to the high thermal diffusion length compared to the skin depth. This depends on the laser fluence, and is measured to be 0.5–3.5 μm.

B. Theoretical results by MD simulation

The temperature distribution in the material in the z direction calculated by the MD simulation is shown in Fig. 5. In this case, the laser fluence is 0.2 J/cm^2 which is above the ablation threshold, and the time from the onset of the laser

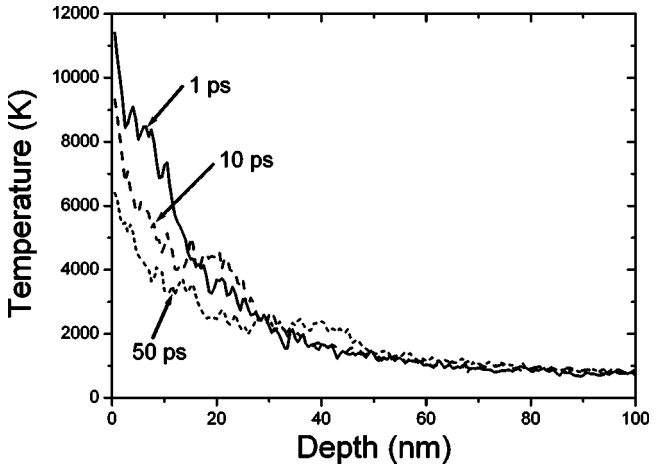

FIG. 5. Temperature distribution in the material at three different times. The laser fluence is 0.2 J/cm^2 and the boiling point T_b and the melting point T_m are 2811 and 1356 K, respectively.

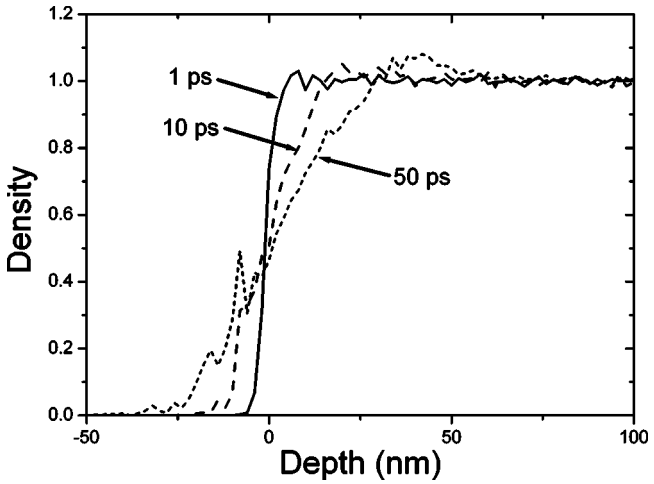

FIG. 6. Dependence of the density on depth and time near the surface.

irradiation is also shown. The relaxation of the temperature begins after 1 ps, while the particles near the surface are quickly heated during the laser irradiation. The strong interaction between the ultrashort laser pulse and the material leads to the formation of a shock wave that propagates into the material. It is found that the temperature distribution has a local maximum under the surface and this peak is transmitted in the material, which is related to the front of the propagated shock wave from the surface.

The dependence of the density on the depth and time near the surface is shown in Fig. 6. The density at $z=0$ after 10 ps becomes small because the ablated particles move near the surface. It is also seen that the density distribution has a maximum under the surface and the wave of condensation and rarefaction occurs due to the shock wave from the surface. The depth of the local maximum of the temperature distribution is the same as that of the maximum of the density distribution.

The dependence of the ablation rate and the heat-affected zone estimated by the MD simulation on laser fluence is shown in Fig. 7. The ablation rate is estimated from the depth which becomes heated above the boiling point T_b (2811 K), and the heat-affected zone is the zone at a temperature between the boiling point T_b and the melting point T_m (1356 K). The ablation rate has two different regimes, as shown in Fig. 7. This is caused by the calculation of the MD simulation taken into account by the two-temperature model. In addition, the thickness of the heat-affected zone at the fluence below the ablation threshold is greater than that at the low fluence over the threshold fluence. The thickness of the heat-affected zone estimated by the MD simulation depends on the laser fluence over the ablation threshold. These are in good agreement with the experimental data.

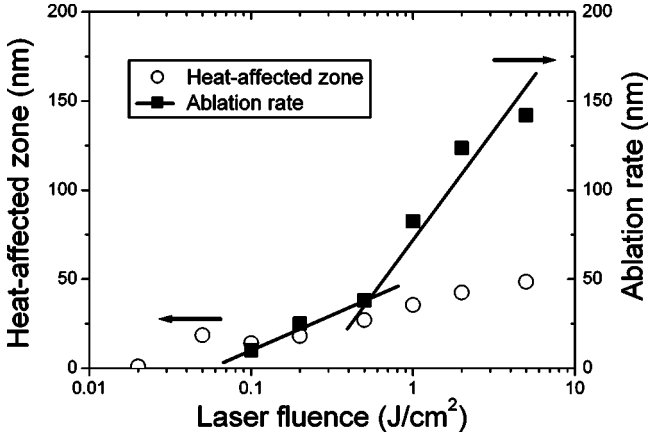

FIG. 7. Ablation rate and heat-affected zone estimated by MD simulation.

The experimental results of the ablation rate and heat-affected zone are consistent with the simulation results (Figs. 4 and 7). The difference in the ablation rate between the experiment and the simulation may be in part due to the fact that the experimental results were taken as an average over many laser shots, while the simulation was performed as a single shot irradiation on a well-defined crystalline surface. The optical parameters of the material, especially the absorption coefficient, may be changed due to the heating up of the laser-irradiated surface. For drilling holes with a higher aspect ratio, in other words, at higher laser fluences, the multiple reflections from the walls and trapping of the ablated material also may decrease the ablation rate.

The thickness of the heat-affected zone calculated by the MD simulation is much smaller than that estimated by the experimental data. This is due to the difference between the single pulse calculation and the multipulse experiment. The defects are formed on the laser-irradiated area, which may change the absorption of the laser energy, the electron excitation, the thermal conduction, and so on. Although the interaction of the next pulse with the materials ablated by the former pulse is not significant due to the repetition rate of 1 kpps, it is difficult to discuss precisely the cumulative effects of the heat-affected zone depending on the pulse number. This is because a new heat-affected zone is formed by the next pulse, after the heat-affected zone formed by the former pulse is ablated partially by the next pulse. It is reported that the thicknesses of the lateral heat-affected zone ablated by the femtosecond laser at 1 kpps repetition rate are 2, and 1.5 μm, respectively, in the case of the thin film[32] and the deformed bulk[33] of aluminum. In addition, the thickness of the heat-affected zone estimated by the MD simulation for the high fluence regime is smaller than the experimental data, because the calculation depth and the calculation time is not enough to prevent the load of the computational calculation from becoming enormous.

V. CONCLUSIONS

The heat-affected zone of Cu ablated with a femtosecond laser was both experimentally and theoretically investigated. As a result of the XRD measurement on the ablated surface, the crystallinity at the surface becomes amorphous partially from the crystal structure. The thickness of the heat-affected zone at a fluence below the ablation threshold is greater than that in the higher fluence regime than the threshold. The heat-affected zone is experimentally observed even with a lower fluence irradiation than the ablation threshold, and at higher laser fluence than the ablation threshold. The heat-affected zone was measured to range from 0.5 to 3.5 μm, which is dependent on the laser fluence.

In addition, the laser ablation of Cu was theoretically investigated by MD simulation coupled with the two-temperature model. The experimental ablation rate and the heat-affected zone are theoretically well explained.

ACKNOWLEDGMENTS

This work is supported partially by a Grant-in-Aid for Scientific Research (Grant No. A15206011) from the MEXT Japan. This work is also supported in part by research fellowships of the Japan Society for the Promotion of Science for Young Scientists.

[1]B. E. Lemoff, G. Y. Yin, C. L. Gordon III, C. P. J. Barty, and S. E. Harris, J. Opt. Soc. Am. B **13**, 180 (1996).
[2]W. K. Kautek and J. Krueger, Proc. SPIE **2207**, 600 (1994).
[3]B. C. Stuart, M. D. Feit, A. M. Rubenchik, B. W. Shore, and M. D. Perry, Phys. Rev. Lett. **74**, 2248 (1995).
[4]E. Takahashi, Y. Nabekawa, T. Otsuka, M. Obara, and K. Midorikawa, Phys. Rev. A **66**, 021802 (2002).
[5]G. L. Eesley, Phys. Rev. B **33**, 2144 (1986).
[6]S. D. Brorson, A. Kazeroonian, J. S. Moodera, D. W. Face, T. K. Cheng, E. P. Ippen, M. S. Dresselhaus, and G. Dresselhaus, Phys. Rev. Lett. **64**, 2172 (1990).
[7]B. C. Stuart, M. D. Feit, S. Herman, A. M. Rubenchik, B. W. Shore, and M. D. Perry, J. Opt. Soc. Am. B **13**, 459 (1996).
[8]B. N. Chichkov, C. Momma, S. Nolte, F. von Alvensleben, and A. Tünnermann, Appl. Phys. A: Mater. Sci. Process. **63**, 109 (1996).
[9]K. Furusawa, K. Takahashi, H. Kumagai, K. Midorikawa, and M. Obara, Appl. Phys. A: Mater. Sci. Process. **69**, S359 (1999).
[10]P. P. Pronko, S. K. Dutta, D. Du, and R. K. Singh, J. Appl. Phys. **78**, 6233 (1995).
[11]R. F. W. Hermann, J. Gerlach, and E. E. B. Campbell, Appl. Phys. A: Mater. Sci. Process. **66**, 35 (1998).
[12]L. V. Zhigilei and B. J. Garrison, Appl. Phys. A: Mater. Sci. Process. **69**, S75 (1999).
[13]P. Lorazo, L. J. Lewis, and M. Meunier, Appl. Surf. Sci. **168**, 276 (2000).
[14]L. V. Zhigilei, P. B. S. Kodali, and B. J. Garrison, J. Phys. Chem. B **102**, 2845 (1998).
[15]E. Ohmura and I. Fukumoto, Int. J. Jpn. Soc. Precis. Eng. **30**, 128 (1996).
[16]P. A. Atanasov, N. N. Nedialkov, S. E. Imamova, A. Ruf, H. Hügel, F. Dausinger, and P. Berger, Appl. Surf. Sci. **186**, 369 (2002).
[17]D. S. Ivanov and V. Zhigilei, Phys. Rev. B **68**, 064114 (2003).
[18]S. Nolte, C. Momma, H. Jacobs, A. Tünnermann, B. N. Chichkov, B. Wellegehausen, and H. Welling, J. Opt. Soc. Am. B **14**, 2716 (1997).
[19]Y. Hirayama, H. Yabe, and M. Obara, J. Appl. Phys. **89**, 2943 (2001).
[20]K. Ozono, M. Obara, A. Usui, and H. Sunakawa, Opt. Commun. **189**, 103 (2001).
[21]Y. Hirayama and M. Obara, J. Appl. Phys. **90**, 6447 (2001).
[22]K. Ozono and M. Obara, Appl. Phys. A: Mater. Sci. Process. **77**, 303 (2003).
[23]A. P. Kanavin, I. V. Smetanin, V. A. Isakov, Yu. V. Afanasiev, B. N. Chichkov, B. Wellegehausen, S. Nolte, C. Momma, and A. Tünnermann, Phys. Rev. B **57**, 14698 (1998).
[24]H. Furukawa and M. Hashida, Appl. Surf. Sci. **197–198**, 114 (2002).
[25]Y. Hirayama and M. Obara, Appl. Surf. Sci. **197–198**, 741 (2002).
[26]S. I. Anisimov, B. L. Kapeliovich, and T. L. Perel'man, Sov. Phys. JETP **39**, 375 (1975).
[27]X. Y. Wang, D. M. Riffe, Y. S. Lee, and M. C. Downer, Phys. Rev. B **50**, 8016 (1994).
[28]M. P. Allen and D. J. Tildesley, *Computer Simulation of Liquids* (Clarendon, Oxford, 1987).
[29]I. A. Girifalco and V. G. Weizer, Phys. Rev. **114**, 687 (1959).
[30]W. C. Swope, H. C. Andersen, P. H. Bernes, and K. R. Wilson, J. Phys. Chem. **76**, 637 (1982).
[31]D. R. Lide, *CRC Handbook of Chemistry and Physics*, 84th ed. (CRC Press, New York, 2003–2004).
[32]R. Le Harzic, N. Huot, E. Audouard, C. Jonin, P. Laporte, S. Valette, A. Fraczewicz, and R. Fortuier, Appl. Phys. Lett. **80**, 3886 (2002).
[33]S. Valette, E. Audouard, R. Le Harzic, N. Huot, P. Laporte, and R. Fortunier, Appl. Surf. Sci. **239**, 381 (2005).